Check for updates

Received: 1 May 2022 | Revised: 7 June 2022 | Accepted: 29 June 2022

DOI: 10.1002/er.8371

RESEARCH ARTICLE

INTERNATIONAL JOURNAL OF ENERGY RESEARCH WILEY

A flexible fiber-shaped hybrid cell with a photoactive gel electrolyte for concurrent solar energy harvesting and charge storage

Tareq Kareri[1,2] | **Mohammad Shakhawat Hossain**[1] | **Manoj K. Ram**[3] | **Arash Takshi**[1,4]

[1]Department of Electrical Engineering, University of South Florida, Tampa, Florida, USA

[2]Department of Electrical Engineering, Najran University, Najran, Saudi Arabia

[3]PolyMaterials App, LLC, Tampa, Florida, USA

[4]Clean Energy Research Center, University of South Florida, Tampa, Florida, USA

Correspondence
Arash Takshi, Department of Electrical Engineering University of South Florida 4202 E Fowler Ave, Tampa, FL 33620, USA.
Email: atakshi@usf.edu

Funding information
National Science Foundation, Grant/Award Number: 1953089

Summary

Fiber-shaped solar energy harvesting and storage devices are promising flexible hybrid systems for next-generation wearable electronics. Here, three flexible fiber-shaped hybrid devices were designed and fabricated by twisting two different conductive threads as electrodes and a photoactive polyaniline (PANI)-based gel electrolyte. For two of the devices, conductive threads, one coated with Ag and another coated with carbon nanotube (CNT), were used as the anode electrodes with different work functions. In the third device, ZnO nanowires (NWs) were grown on the CNT coated threads as the electron transport layer (ETL) on the anode. The highest capacitance was found to be 10.1 mF cm^{-1} (69.7 mF g^{-1}) in device with the anode made of Ny66-Ag/CNT, while a photovoltage of 37 mV was measured in the device with the ETL when exposed to light for 400 s. The current results provide a new design strategy with a flexible structure and simple fabrication process for the fiber-shaped hybrid devices with the dual properties of energy harvesting and storage.

KEYWORDS

fiber-shaped devices, photoactive electrolyte, threads, wearable electronics, zinc oxide nanowires

1 | INTRODUCTION

Science is making rapid steps towards the era of artificial intelligence and the internet of things to provide an intelligent future that can enhance the speed, accuracy, and effectiveness of research, human, and industrial efforts. In this process, the new generation of electronics must keep pace with this development and comply with the requirements in terms of shape, flexibility, functionality, and performance for the new applications. Currently, majority of the wearable electronics are made of circuits being fabricated on a flexible substrate and glued/sewn to fabrics.[1] Such structures lack the required flexibility for convenient wearable electronics. Hence, the focus is drifting towards fiber-based devices and systems that can be integrated into fabrics. Considering the required powers for such electronics, fiber-shaped supercapacitors and fiber-shaped solar cells have attracted increasing scientific attention.[2,3] Various types of fiber-shaped supercapacitors have been reported in recent years with parallel,[4,5] twisted,[6] and coaxial fiber structures[7,8] fabricated with different methods using various types of the electrode materials (ie, carbon-based,[7] metallic,[4] and composite materials).[5,6,9] Some of the devices have presented

 © 2022 John Wiley & Sons Ltd.

1099114x, 2022, 12, Downloaded from https://onlinelibrary.wiley.com/doi/10.1002/er.8371 by Health Science Center, Wiley Online Library on [15/01/2023]. See the Terms and Conditions (https://onlinelibrary.wiley.com/terms-and-conditions) on Wiley Online Library for rules of use; OA articles are governed by the applicable Creative Commons License

relatively high power densities, fast charging/dis-charging, and long cycle life. However, the low energy density and high self-discharge in such devices are among challenges that require more scientific studies.[10] Also, energy harvesting devices (eg, solar cells) can be fabricated using fibers and threads. Different types of fiber-shaped solar cells have been reported recently, such as dye-sensitized solar cells,[11,12] perovskite,[13] and organic solar cells.[14] Due to the growing interests in this field, in the recent years, several review papers have been published in the field of fiber-shaped electronic devices and wearable solar cells.[3,15]

Integrating electrochemical energy storage and harvesting in a single fiber-based hybrid device presents unique features and potential for wearable applications and self-powered systems. However, some issues and challenges need to be overcome, such as low efficiency and performance, low mechanical and electrochemical stability, and cost of fabrication.[2] Although the majority of the reported hybrid devices for wearable electronics were made with flat structures stacking solar cells and supercapacitors being attached to textile,[16] some devices used conductive threads as the electrodes to make fiber shape supercapacitors and solar cells connected together to make a hybrid system.[17] Dye-sensitized solar cells are widely used as an energy conversion unit in most fiber-shaped hybrid devices due to their low cost, reasonable efficiency, and ease of fabrication, and they can be fabricated with the energy storage unit on the same thread (electrode)[18,19] or different threads separately, which can be woven into textiles.[20] However, the complexity in fabricating solar cells and supercapacitors on threads is a major concern for their applications in wearable electronics.

In the attempt for developing two-terminal hybrid solar cell-supercapacitor devices, previously, we have reported a new class of hybrid devices made from a photoredox active gel electrolyte being placed between two electrodes.[21] The gel was a composite material consisting of polyvinyl alcohol (PVA), polyaniline (PANI), ammonium persulfate (APS), and an acid. The fabrication process of the flat devices was as simple as placing the photoredox active gel electrolyte between two electrodes.[21-23] In this work, the approach has been transformed for making thin, lightweight, and flexible fiber-shaped hybrid energy storage and harvesting devices with a twisted structure and simple fabrication processes using two conductive threads and the photoactive composite gel electrolyte. Although the gel electrolyte functionality, which can serve both as a redox-active layer and electrolyte, is critical to develop a hybrid device, the work function and structure of the electrodes are also important for efficient charge storage and electron transfer. Hence, we have studied the effect of the different anode thread shape electrodes in devices made with a stainless steel (SS) fiber shape cathode and the composite gel electrolyte. Three devices were fabricated and compared. The first device was made using a silver-coated nylon 66 (Ny66-Ag) thread and a CNT coated Ny66-Ag thread was used as the anode in the second device. To improve the electron transfer rate from the gel to the anode, the third device had an anode made from a CNT coated thread with a grown layer of ZnO NWs (Ny66-Ag/CNT/ZnO-NWs) as the electron transport layer.

2 | RESULTS AND DISCUSSION

2.1 | Device fabrication and characterization

The fiber-shaped hybrid devices were fabricated by cutting 10 cm long pieces of the prepared anode electrodes (Ny66-Ag, Ny66-Ag/CNT, or Ny66-Ag/CNT/ZnO-NWs threads) and a similar size cathode electrode (SS-based conductive thread), covering separately by a uniform thin layer of the PVA/PANI composite gel electrolyte, and drying for 24 h at room temperature. Then, the devices were made by putting the anode and cathode electrodes in parallel with a few millimeters spacing, applying a layer of the gel electrode between them and then twisting the threads for 10 turns (~1 turn per cm). Figure 1 shows the simple steps used for fabricating a device and pictures of hybrid devices tested in the lab.

To understand the surface morphology of the fiber-shaped electrodes, scanning electron microscopy (SEM) images were taken before coating with the gel and the device fabrication. Figure 2A shows an SEM micrograph of the commercial conductive Ny66-Ag thread with an estimated diameter of 560 μm. Also, it can be seen that the microfibers have a uniform structure with ~29 μm in diameter for each fiber (Figure 2B).

Also, it can be seen that the microfibers have a uniform structure with ~29 μm in diameter for each fiber (Figure 2B). The diameter of the Ny66-Ag/CNT thread remained uniform after coating the Ny66-Ag thread with a layer of CNT, as shown in Figure 2C,D. Figure 2E,F exhibit the surface of the Ny66-Ag/CNT/ZnO-NWs electrode after the hydrothermal growth of ZnO nanowires. The thread was uniformly covered with radially aligned ZnO nanowires with an estimated nanowire length of 2 μm and diameter of 330 nm. For the cathode electrode, SS thread with a diameter of ~490 μm (Figure 2G) and

10991114x, 2022, 12, Downloaded from https://onlinelibrary.wiley.com/doi/10.1002/er.8371 by Health Science Center, Wiley Online Library on [15/01/2023]. See the Terms and Conditions (https://onlinelibrary.wiley.com/terms-and-conditions) on Wiley Online Library for rules of use; OA articles are governed by the applicable Creative Commons License

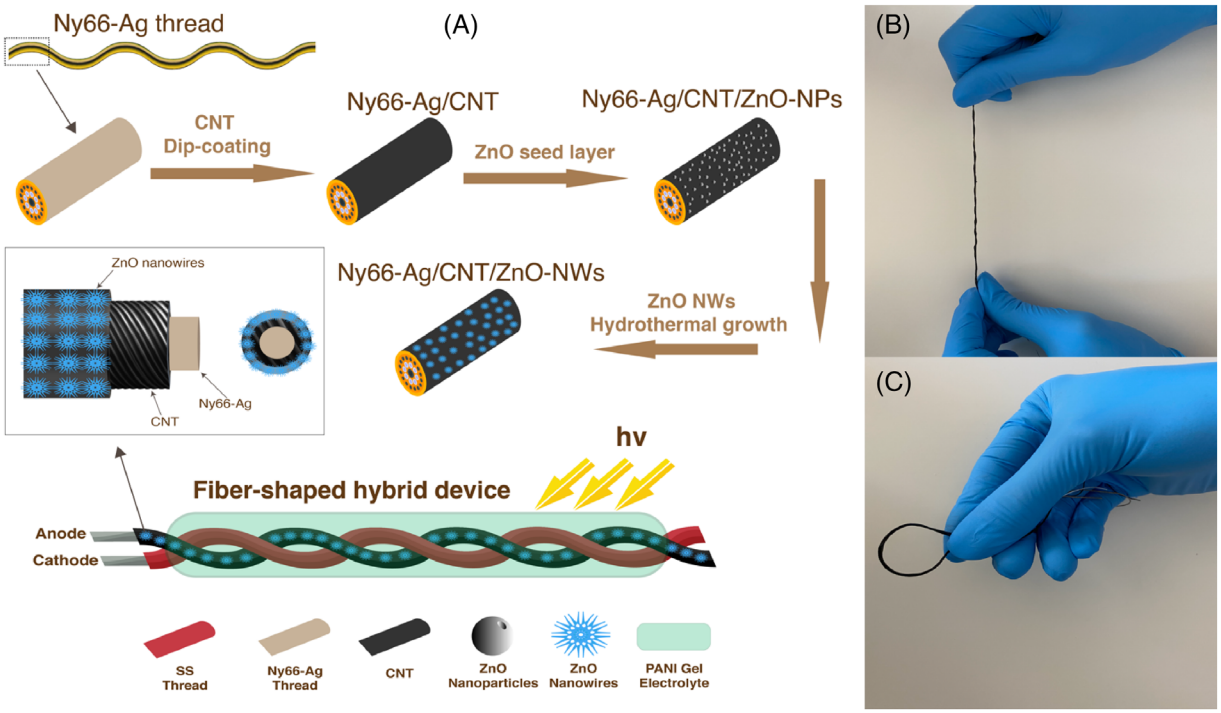

FIGURE 1 (A) Schematic illustration of the fabrication steps of the Ny66-Ag/CNT/ZnO-NWs anode electrode and the final device structure. (B, C) Photographs of the fiber-shaped hybrid devices

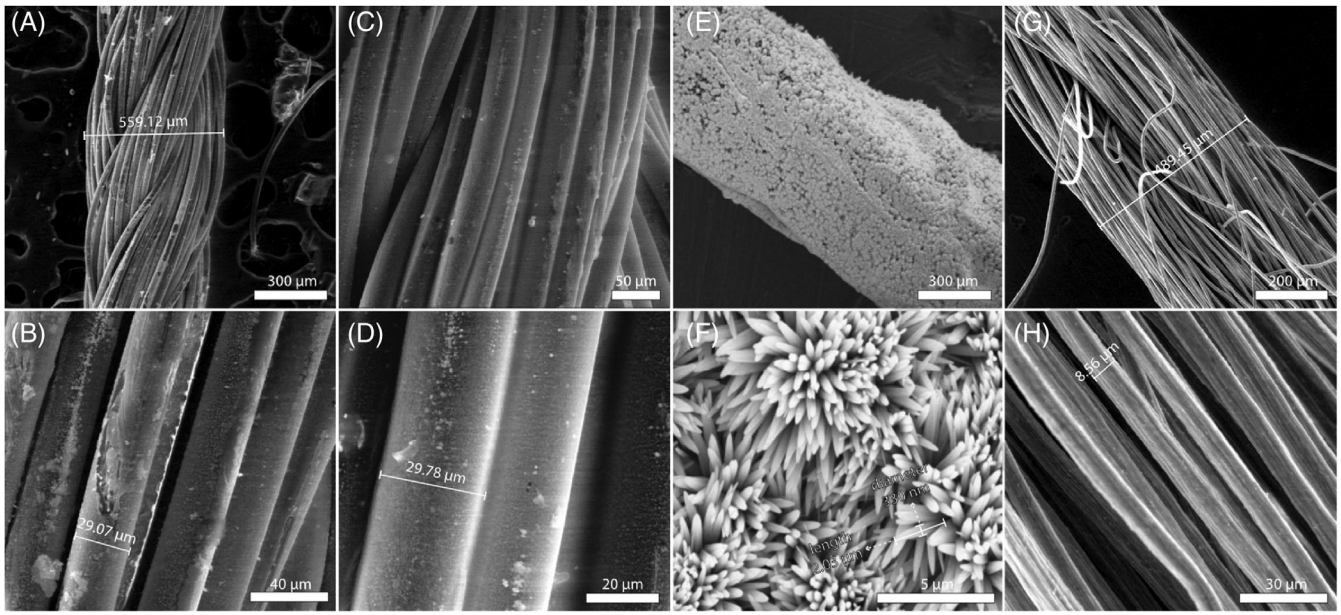

FIGURE 2 Morphological characterization of electrodes. SEM images of (A, B) Ny66-Ag conductive thread at different magnifications, (C, D) Ny66-Ag/CNT electrode surface, (E, F) ZnO nanowires growth on Ny66-Ag/CNT/ZnO-NWs electrode, (G, H) SS conductive thread at different magnifications

~ 8.5 µm for each fiber (Figure 2H) was used. Furthermore, energy-dispersive X-ray spectroscopy (EDS) analysis was conducted to identify the chemicals on the anode electrodes. The result in Figure 3A confirms the presence of a high percentage of Ag element (~75 wt%) in the Ny66-Ag conductive thread. After adding a CNT layer uniformly on the surface of the Ny66-Ag, carbon and Ag elements appeared in the spectrum with percentages of 48.8 and 50.1 wt% respectively (Figure 3B). Meanwhile, the elements sodium (Na) and sulfur (S) also appeared

10991 14x, 2022, 12, Downloaded from https://onlinelibrary.wiley.com/doi/10.1002/er.8371 by Health Science Center, Wiley Online Library on [15/01/2023]. See the Terms and Conditions (https://onlinelibrary.wiley.com/terms-and-conditions) on Wiley Online Library for rules of use; OA articles are governed by the applicable Creative Commons License

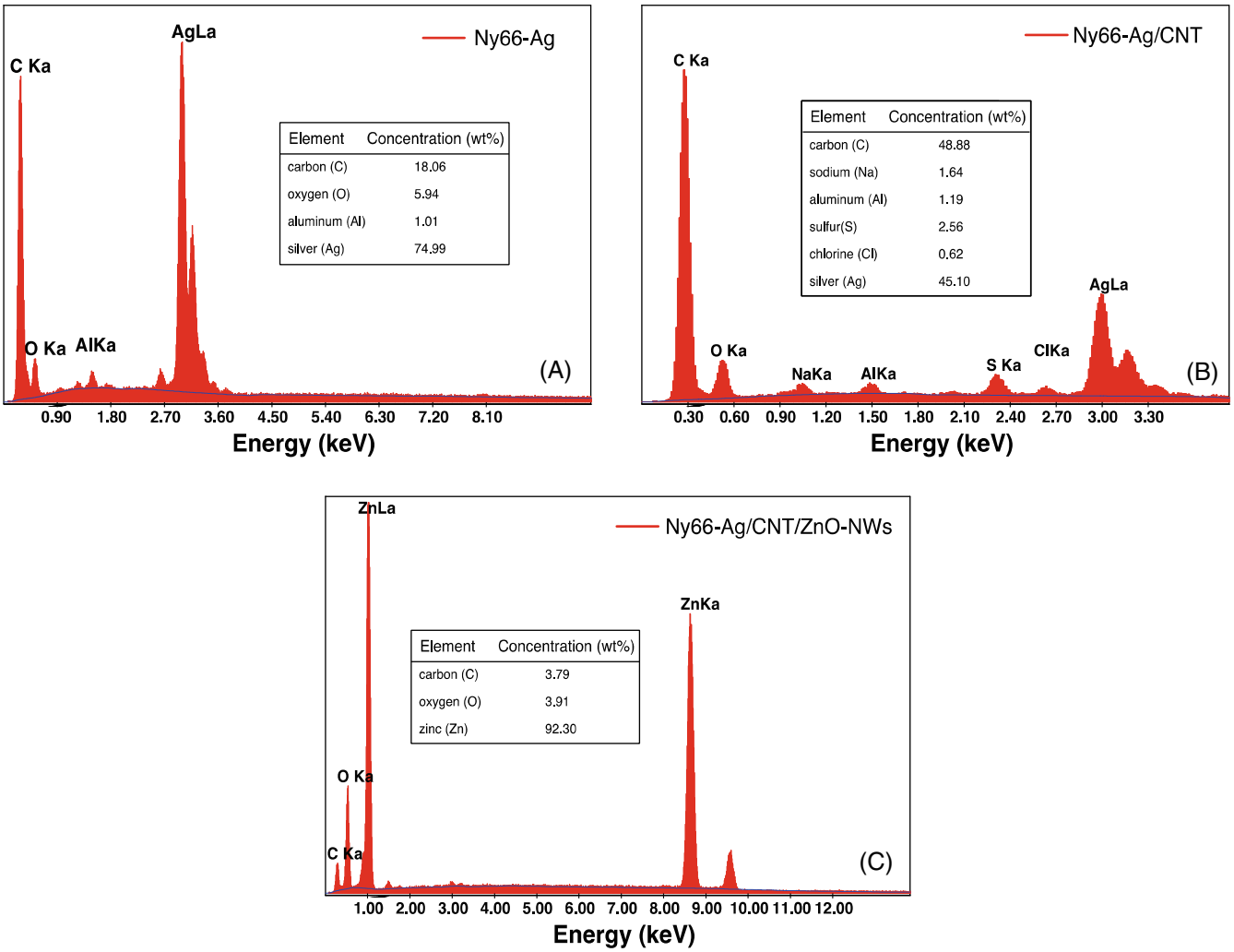

FIGURE 3 Energy-dispersive X-ray spectroscopy (EDS) analysis of (A) Ny66-Ag conductive thread, (B) Ny66-Ag/CNT, and (C) Ny66-Ag/CNT/ZnO-NWs electrodes.

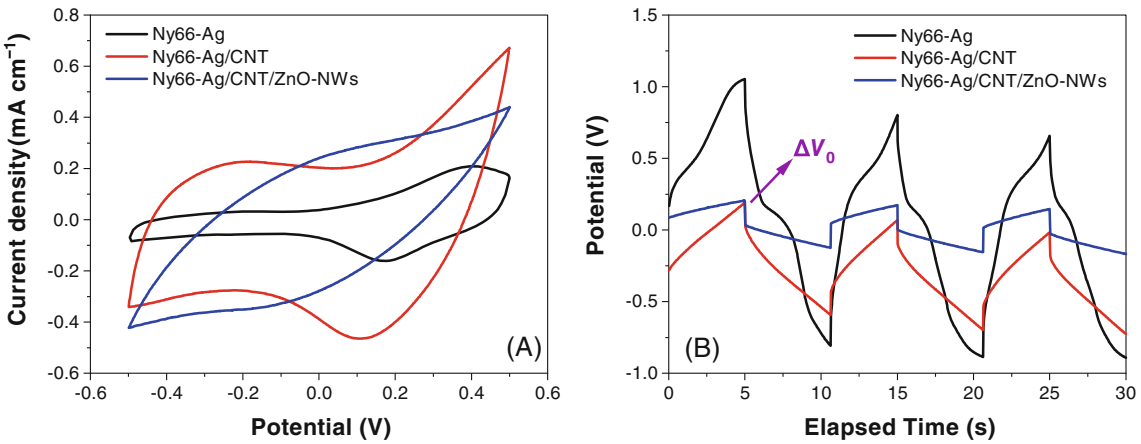

FIGURE 4 Comparative (A) cyclic voltammetry (CV) and (B) galvanostatic charge-discharge curves of the fiber-shaped hybrid device with Ny66-Ag, Ny66-Ag/CNT, and Ny66-Ag/CNT/ZnO-NWs anode electrodes tested in dark. The CV scan rate was 50 mV s^{-1}

due to adding sodium dodecylbenzenesulfonate (SDBS) surfactant with the CNT ink. The EDS analysis of the Ny66-Ag/CNT/ZnO-NWs electrode indicates a high percentage of Zn, about 92.3 wt%, confirming the homogeneous coverage of the thread surface with the ZnO nanowires (Figure 3C)

10991141x, 2022, 12, Downloaded from https://onlinelibrary.wiley.com/doi/10.1002/er.8371 by Health Science Center, Wiley Online Library on [15/01/2023]. See the Terms and Conditions (https://onlinelibrary.wiley.com/terms-and-conditions) on Wiley Online Library for rules of use; OA articles are governed by the applicable Creative Commons License

2.2 | Electrochemical properties of fiber-shaped hybrid devices

The fabricated devices were characterized using various electro-chemical experiments. Cyclic Voltammetry (CV) measurements were executed with the potential range between −0.5 and 0.5 V at 50 mV s^{-1} scan rate to investigate the energy storage performance of the fiber-shaped hybrid devices. As shown in Figure 4A, the CV curve from the first device with the anode of Ny66-Ag showed energy storage capability with both double-layer and pseudocapacitive charge storage mechanisms with redox peaks at 0.2 and 0.4 V. A similar effect of pseudo-capacitive storage was observed in our previous work when twisted-fiber supercapacitors were made from a PVA-based gel and two Ny66-Ag electrodes with the strong redox peaks associated to silver.[24] Knowing the length of the threads (ie, devices) and considering the devices as a cylinder with a measured diameter of ∼1 mm, the length, area, and volume-specific capacitance of the fiber-shaped hybrid device with the Ny66-Ag electrode were calculated in the dark to be 2.9, 29 mF cm^{-2}, and 370.2 mF cm^{-3} (20.2 mF g^{-1}) respectively. The device exhibited a volumetric energy density of 0.22 mW h cm^{-3}. As expected, after coating the threads with CNTs, the specific capacitance of the Ny66-Ag/CNT device was increased to 10.1 mF cm^{-1} (69.7 mF g^{-1}) with a volumetric energy density of 0.73 mW h cm^{-3} likely due to the much larger surface area that CNTs have provided. The CV curves of Ny66-Ag/CNT electrode also show a two-stage charge storage mechanism with shifting the anodic peak to 0.1 V and the cathodic peak to a voltage higher than 0.5 V. Since MWCNTs and stainless steel are not redox active materials, the strong peaks can be due to the redox reactions because of the change in the oxidation state of PANI between the emeraldine salt (ES) and the leucoemeraldine salt (LS) states ($ES + 2ne- + 2nH+ \leftrightarrows LS$) inside the gel as reported before.[21] However, the change in the cell resistance after coating with CNTs can be the reason for shifting the redox peaks in the two-terminal electrochemical cell. After ZnO nanowires growth on the Ny66-Ag/CNT/ZnO-NWs electrode, the device showed a dominated double-layer charge storage with no redox peaks which is likely due to the thick layer of ZnO NWs and their semiconducting property suppressing reversible redox reactions at the anode.[25] Accordingly, the calculated specific capacitance and volumetric energy density were 6.8 mF cm^{-1} (47.4 mF g^{-1}) and 0.5 mW h cm^{-3} respectively. As the results suggest, the Ny66-Ag/CNT fiber delivers the highest volume-specific capacitance of 1.27 F cm^{-3} (69.7 mF g^{-1}), compared to the other electrodes. Also, each device was tested once in the dark and once under solar simulated illumination. All three devices showed a slight increase in the capacitance under illumination, indicating the solar energy harvesting and energy storage capabilities of the gel electrolyte (Figure S1). However, due to the domination of the capacitive effect, the current-voltage characteristic in the devices are almost the same with a small increase in the voltage and current in the light, due to the generated photovoltage and photocurrent.

To understand the effect of different coatings on the series resistance (R_s), the galvanostatic charge-discharge profiles of the fiber-shaped hybrid devices were studied by chrono-potentiometry (CP) method at a constant current of ±500 μA for Ny66-Ag and Ny66-Ag/CNT, and ± 50 μA for Ny66-Ag/CNT/ZnO-NWs. The charge-discharge curves shown in Figure 4B exhibit non-linear shapes for Ny66-Ag and Ny66-Ag/CNT electrodes during the charging and discharging cycles due to the faradaic reaction.[24] However, the Ny66-Ag/CNT/ZnO-NWs electrode shows an almost linear voltage profile during the charging and discharging cyclFes, confirming the observed double-layer charge storage mechanism in the CV results.[26] Considering the voltage drop (ΔV_0) at the transition between the charging and discharging cycles, the equivalent series resistance (ESR) of the devices were found to be 102.46, 111.68, and 1733.3 Ω for the devices with the anode of Ny66-Ag, Ny66-Ag/CNT, and Ny66-Ag/CNT/ZnO-NWs respectively.

As shown in Figure S2, due to the domination of the capacitive effect, the standard I-V characterization for solar cells does not reflect the ability of the hybrid 2-terminal devices.[27] Therefore, the open circuit potential (OCP) and short circuit current (SCC) measurements were conducted to gain further insights into the photovoltaic (PV) performance of the fiber-shaped hybrid devices. As illustrated in Figure 5A, OCP of the fiber-shaped hybrid devices was tested with the different anode electrodes in two steps, under illumination for 400 s and in the dark for 600 s. In all devices, the magnitude of the OCP increased during the illumination, confirming the ability of harvesting energy. The negative photovoltage implies electron collections by the anode. For the Ny66-Ag electrode, the magnitude of the photovoltaic potential (ΔV_{ph}) was increased around 30 mV under illumination and slightly decreased to ∼28 mV in the dark mode. However, after adding a porous layer of CNT on the electrode (Ny66-Ag/CNT), the voltage of the hybrid device only reached 17 mV in light with a high self-discharge rate in the dark. As expected, the highest OCP was achieved after adding the electron transport layer (ZnO NWs) on the electrode. The photovoltage was improved significantly and reached 37 mV in 400 s of illumination in the device with the Ny66-Ag/CNT/ZnO-

10991 14x, 2022, 12, Downloaded from https://onlinelibrary.wiley.com/doi/10.1002/er.8371 by Health Science Center, Wiley Online Library on [15/01/2023]. See the Terms and Conditions (https://onlinelibrary.wiley.com/terms-and-conditions) on Wiley Online Library for rules of use; OA articles are governed by the applicable Creative Commons License

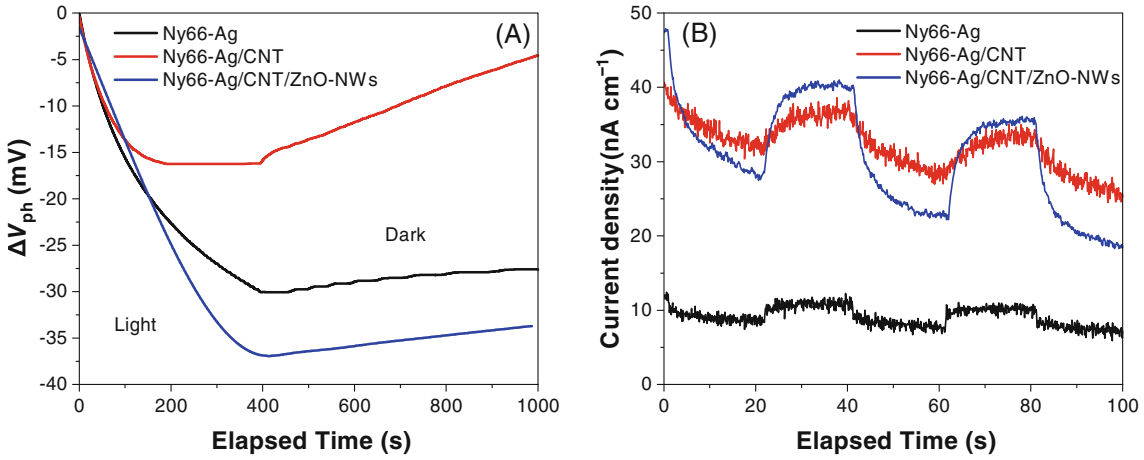

FIGURE 5 Comparative measurements of (A) open circuit potential of the fiber-shaped hybrid devices with Ny66-Ag, Ny66-Ag/CNT, and Ny66-Ag/CNT/ZnO-NWs anode electrodes and (B) short circuit current under light pulses

NWs electrode. The power conversion efficiency (η) of the devices was calculated as output power (P_{out})/input power (P_{in}), where P_{out} = stored energy/charging time, and P_{in} = light intensity × area. The stored energy was calculated as $1/2C(\Delta V_{ph\text{-}max})^2$, where C is the capacitance of the device and $\Delta V_{ph\text{-}max}$ is the maximum photovoltaic potential. Accordingly, the device with the Ny66-Ag/CNT/ZnO-NWs electrode achieved a cell efficiency of 0.5% compared with 0.043% and 0.036% for the Ny66-Ag and the Ny66-Ag/CNT electrode respectively. It should be mentioned that due to the hybrid design of the cell the efficiency is expected to be lower than a non-hybrid device.[27] Also, it should be considered that the thread-shaped design cannot harvest photons as efficiently as a planar structure. But the internal energy storage is an advantage for wearable applications where a thread may not receive a uniform light exposure. Nevertheless, the conversion efficiency with the ZnO-NWs is promising for further optimization.

Besides, SCC measurements were executed under light pulses to evaluate the photocurrent response in the fiber-shaped hybrid device. Since the thickness of the twisted structures were almost the same in all three different devices (~1 mm), the current density is reported as the normalized current to the device length, as depicted in Figure 5B. Under illumination cycles, the fiber-shaped hybrid device exhibited a photocurrent (ΔI) response around 3.5, 6.3, and 15.1 nA cm^{-1} with the Ny66-Ag, Ny66-Ag/CNT, and Ny66-Ag/CNT/ZnO-NWs electrode respectively. The good repeatability after several cycles of light pulses suggests the stability of the light response. The results clearly show that after adding the ETL of ZnO NWs, the photocurrent was improved significantly. It should be noted that the negative OCP and positive photocurrent implies the generation mode in all devices.[28]

Electrochemical impedance spectroscopy (EIS) measurements were conducted to study the behavior of the interface between the electrodes and the electrolyte in the devices. The EIS experiments were conducted in a frequency range of 10 kHz to 0.1 Hz at 0 V DC bias and a sinusoidal signal of 15 mV. Figure 6 exhibits the Nyquist plots of the fiber-shaped hybrid devices under the dark and light conditions. The impedance results of the devices with the Ny66-Ag and Ny66-Ag/CNT electrodes showed relatively small series resistances at the high frequency compared to R_s in the Ny66-Ag/CNT/ZnO-NWs electrode. At lower frequencies, the diffusion tail slope for all electrodes revealed an inclination of almost 45°. To compare the differences in different electrodes under the dark and light conditions, a simple electrochemical equivalent circuit was suggested. The measured EIS spectra were fitted to the simulated model using EIS Spectrum Analyser software based on the proposed equivalent circuit in Figure 6D, representing the two-stage charge storage mechanism at the electrode-electrolyte interface (C_{dl}) and in the bulk of the gel electrolyte (C_g).[22] The equivalent circuit model is also described by the series resistance of the device (R_s), the resistance of the photoactive gel electrolyte (R_g), and the constant phase element (*CPE*). The fitting parameters are listed in Table S1 (Supporting Information). Comparing the results in Figure 6A-C, it was observed that the effect of illumination on the impedance in the devices with the Ny66-Ag and Ny66-Ag/CNT electrodes was not significant, while a noticeable change was found in R_s with the Ny66-Ag/CNT/ZnO-NWs electrode under illumination. In that device, R_s dropped from 1733.3 Ω in the dark to 1713.4 Ω under simulated solar illumination. As it is obvious in Figure 6D, the R_s value in the Ny66-Ag/CNT/ZnO NWs is one order of magnitude higher than the other two devices due to the ZnO NW coating with a higher resistance than CNT.

The stability of the nonencapsulated device with ZnO NWs was further studied by testing it 4 mo after the

10991146x, 2022, 12, Downloaded from https://onlinelibrary.wiley.com/doi/10.1002/er.8371 by Health Science Center, Wiley Online Library on [15/01/2023]. See the Terms and Conditions (https://onlinelibrary.wiley.com/terms-and-conditions) on Wiley Online Library for rules of use; OA articles are governed by the applicable Creative Commons License

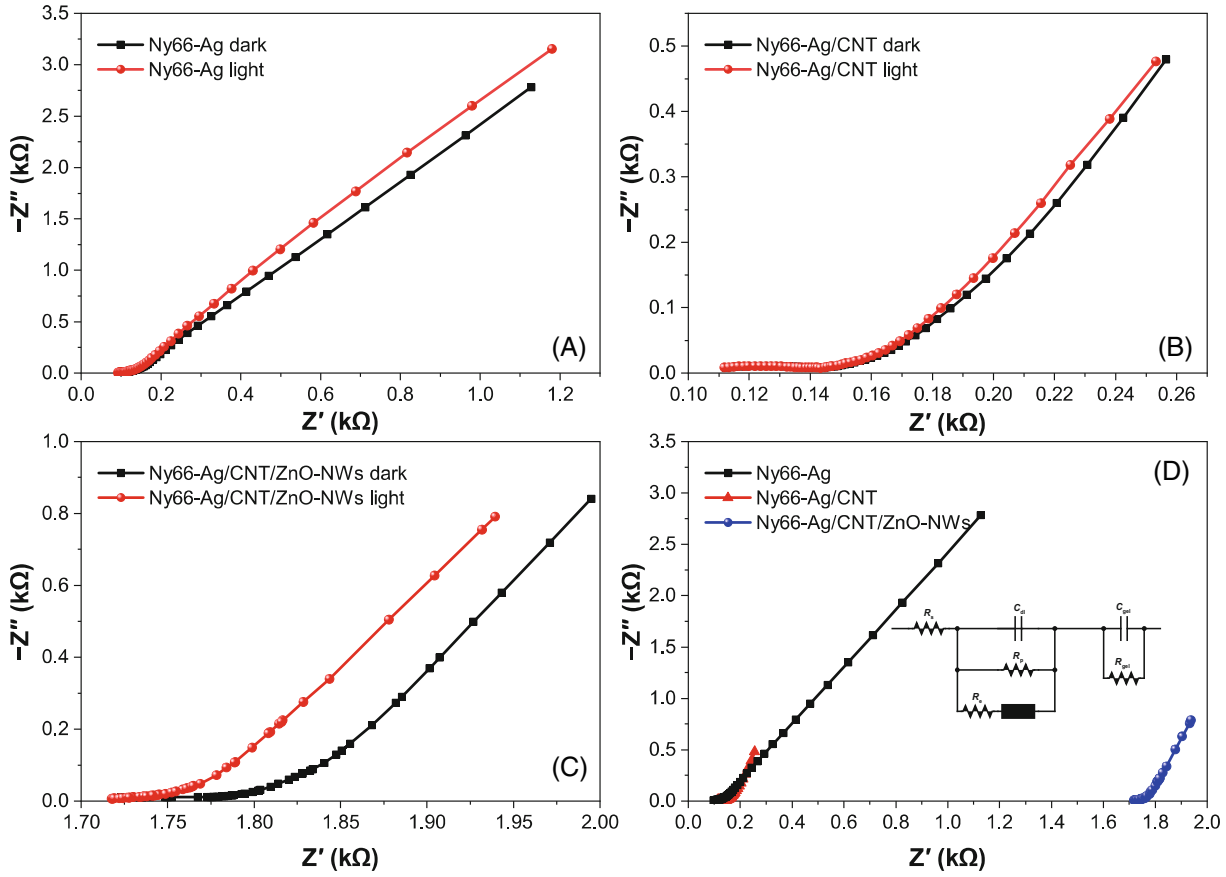

FIGURE 6 Nyquist plots of the fiber-shaped hybrid device with (A) Ny66-Ag, (B) Ny66-Ag/CNT, and (C) Ny66-Ag/CNT/ZnO-NWs anode electrodes in the dark and under illumination. (D) Comparative Nyquist plots of the devices in the dark condition. (Inset) the equivalent circuit model.

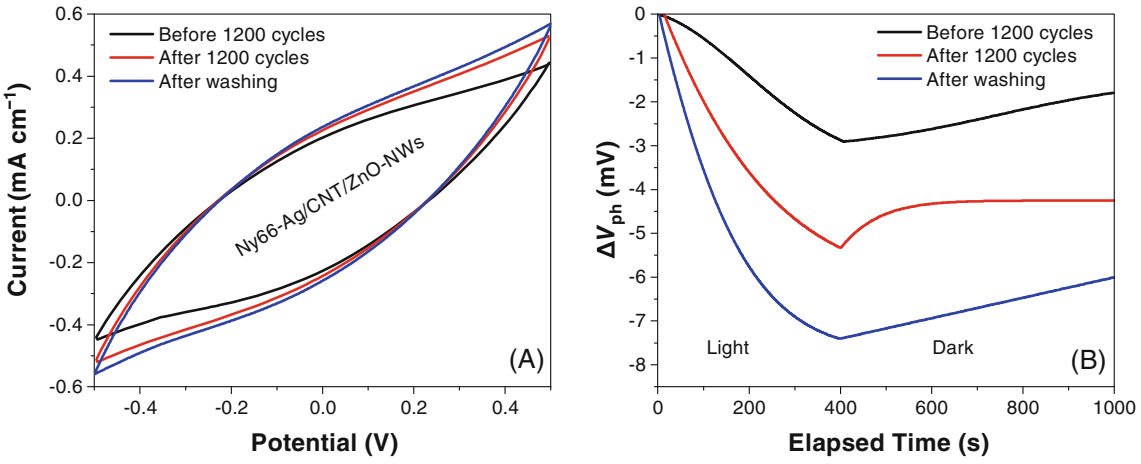

FIGURE 7 Stability measurements of the nonencapsulated device with the Ny66-Ag/CNT/ZnO-NWs electrode after 4 mo of storage in the lab. (A) cyclic voltammetry curves before/after 1200 cycles at 50 mV s^{-1} and after the washing process. (B) Photovoltaic performance during the stability measurements

fabrication while being stored in the lab. Following the test, the device was charged and discharged for 1200 cycles with a scan rate of 50 mV s^{-1}. The performance of the device was tested again after the cycles. The results of the CV and the OCP measurements are presented in Figure 7. While the capacitance was 6.8 mF cm^{-1} (0.87 F cm^{-3} or 47.4 mF g^{-1}), (Figure 4A), the CV result in Figure 7A shows a drop in the

10991 14x, 2022, 12, Downloaded from https://onlinelibrary.wiley.com/doi/10.1002/er.8371 by Health Science Center, Wiley Online Library on [15/01/2023]. See the Terms and Conditions (https://onlinelibrary.wiley.com/terms-and-conditions) on Wiley Online Library for rules of use; OA articles are governed by the applicable Creative Commons License

capacitance to 5.6 mF cm^{-1} (0.71 F cm^{-3} or 38.7 mF g^{-1}) after being stored for 4 mo. However, after 1200 cycles of charging and discharging, the capacitance was increased to 6.3 mF cm^{-1} encouraging frequent use of the device to maintain the original energy storage capability. Since the device was not sealed, there was a question if the degradation in the device performance was due to the loss of water in the composite gel over the storage time. Therefore, after the cycling test, the device was soaked in DI water and left for a day to dry before testing.

The experiment was conducted to find the effect of exposing the sample to water in a washing process for wearable electronics. The CV results showed an increase in the capacitance to 6.7 mF cm^{-1} (0.85 F cm^{-3} or 46.3 mF g^{-1}) which was almost as high as the original capacitance of 6.8 mF cm^{-1} (47.4 mF g^{-1}). The effect of aging, cycling, and washing on the photovoltaic performance of the cell was studied through the OCP measurement in Figure 7B. Unfortunately, the photovoltaic response was significantly weaker after 4 mo storage resulting in only $\Delta V_{ph} = \sim 2.8$ mV. Similarly, after 1200 cycles of charging and discharging (CV in dark), the performance was slightly improved to achieve an OCP of 5.4 mV. Further increase (by 37%) was observed after the washing process. However, the overall photovoltaic effect was much weaker than the original performance. At this point, it is not clear why after 1200 cycles of charge-discharge the capacitance and ΔV were slightly increased. Further studies are required for a better understanding of the mechanisms affecting the shelf-life, cycle-life, and washability of the device. Particularly, for real applications, the effect of washing the sample with water containing minerals (tap water) and detergent while scrubbing the sample has to be investigated.

The mechanisms of charge generation in the bulk gel and unidirectional charge transport through the hybrid device are similar to those in bulk heterojunction organic solar cells,[29] where the photogenerated charges diffuse toward electrodes and due to the difference in the work function of the electrodes or application of electron/hole transport layers, the charges are selectively collected by the anode and cathode. However, in the hybrid cell, instead of electrons and holes, there are electronic and ionic charges. Recombination also occurs between the ionic and electronic charges. In order to understand the correlation between the energy structure of the materials and the energy harvesting, the energy levels of the cathode, PANI, APS, and the anode before and after adding the CNT layer and ZnO NWs were considered. Figure 8 illustrates the comprehensive energy diagram of the devices. The gel is a composite material. However, since PVA is not a conductive material and H_3PO_4 is acting as the supporting electrolyte, we have considered the energy levels in PANI and the electrochemical potential of APS. Chemical polymerization of aniline in presence of APS and an acid produces PANI in its emeraldine salt (ES) state.[30] Based on the two peaks in the UV-vis absorption spectrum of the gel (Figure S3), the energy levels in the PANI is expected to have a polaron state 2.8 eV lower than the lowest unoccupied molecular orbital (LUMO).[21] As shown in Figure 8, absorption of photons can promote electrons from lower states to the LUMO level. Persulfate anion acts as a mediator between PANI and the cathode by interacting with the lost electrons in the lower states in PANI and receiving electrons from the cathode (work function of −4.5 eV)[31] in a reversible reaction ($S_2O_8^{2-} + 2e^- \leftrightarrow 2SO_4^{2-}$). While the transfer of electrons from the cathode to the PANI is expected to be the same in all three devices, it is expected that the electron transfer from the gel to the anode to be different for different anodes. Considering both Ny66-Ag and Ny66-Ag/CNT as conductors, the energy structure of them are shown with their work function (Φ_{WF}) at −4.3 eV for Ag[32] and −4.8 eV for CNT.[33-35] In the absence of an electron transport layer between the photoactive materials (ie, the gel) and the anode in the first two devices, the electron transfer to the anode is expected to be inefficient, due to the high rate of recombination in the electrode-electrolyte interface. However, considering the work function of the cathode electrode ($\Phi_{WF, SS} = -4.5$ eV), the lower work function of the anode, after deposition of CNT, has decreased the photovoltaic performance, which can be observed in the open circuit voltage results. In order to improve the light harvesting and electron extraction efficiency in the hybrid device, ZnO nanowires were grown on the CNT layer as an electron transport layer (ETL). Due to the semiconducting properties of ZnO with the conduction band edge at $E_{CB} = -4.2$ eV and the valence band edge at $E_{VB} = -4.7$ eV,[36,37] a rectifying mechanism is established for transferring the excited electrons from the gel to the anode and block the recombination of the holes at the anode surface.[38,39] The presence of the ETL clearly led to boosting the photovoltaic performance with higher OCP and photocurrent (Figure 5). Considering the gel as a conductor for both electronic (through PANI) and ionic charges (through anions and cations), optimizing the performance of a hybrid device is challenging. However, improving the performance after washing the device indicates the importance of ionic charge transportation through the gel. The results clearly show the feasibility of fabricating simple thread-shape hybrid devices using photo-redox active gels with comparable energy storage capacitances to the conventional supercapacitors. Although, potentially, thread-shaped two-terminal hybrid cells are suitable for low-voltage and low-power wearable

10991114x, 2022, 12, Downloaded from https://onlinelibrary.wiley.com/doi/10.1002/er.8371 by Health Science Center, Wiley Online Library on [15/01/2023]. See the Terms and Conditions (https://onlinelibrary.wiley.com/terms-and-conditions) on Wiley Online Library for rules of use; OA articles are governed by the applicable Creative Commons License

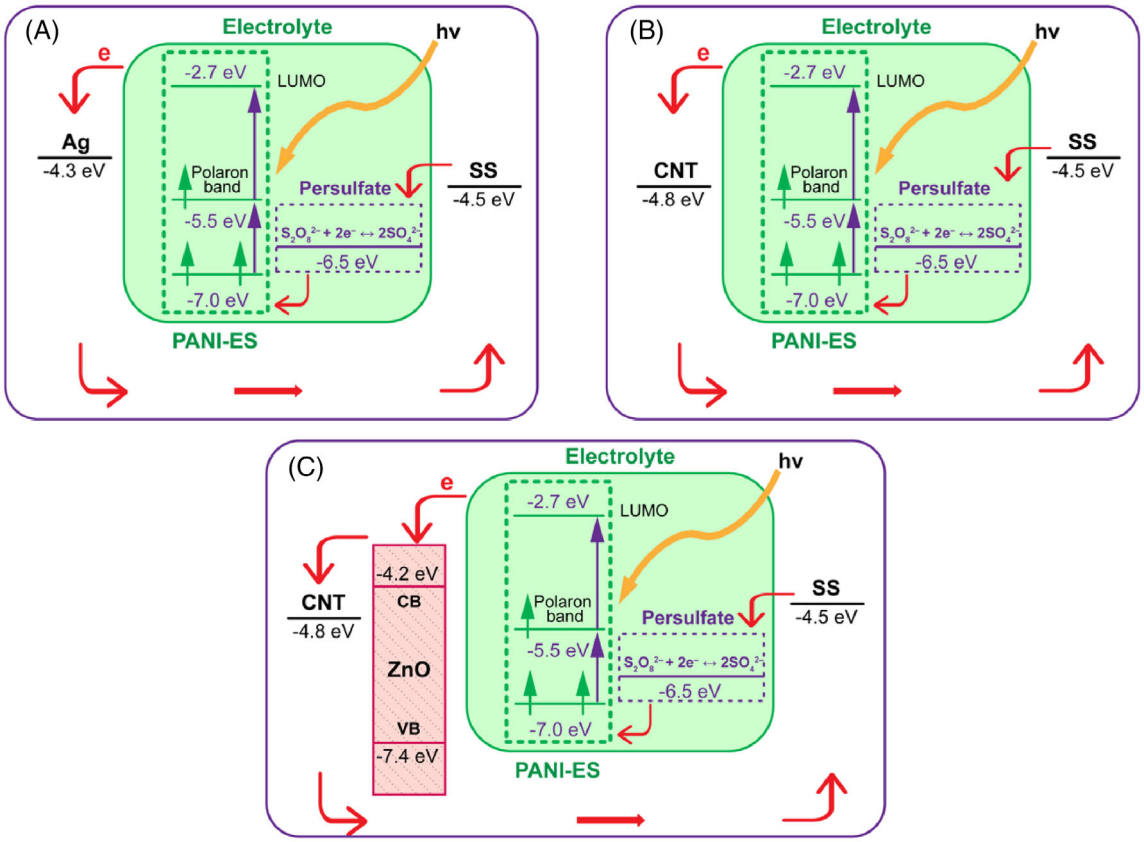

FIGURE 8 Energy diagram of the fiber-shaped hybrid device with (A) the Ny66-Ag, (B) Ny66-Ag/CNT, and (C) the Ny66-Ag/CNT/ZnO-NWs electrode

electronics,[27] significant improvement in the photovoltaic performance of the device is required before using them in practical applications. A simple solution is to add a dye material to the gel. However, as the concept of two-terminal hybrid devices has been discussed in detail in our previous publication,[27] there is a strong correlation between the devices' structure and their electrical and photovoltaic properties. Hence, detailed studies, including photoluminescence and fluorescence studies, will be required to understand the interaction between dye molecules and PANI. More importantly, the effect of improving the photovoltaic properties on the energy storage has to be investigated.

3 | CONCLUSION

In conclusion, a fiber-based hybrid device design consisted of two conductive threads and a photoactive gel electrolyte with the photoelectric and energy storage properties has been demonstrated. The experimental results indicate that the PANI-based photoactive gel electrolyte can be used for fiber-shaped hybrid devices with a simple fabrication process. The energy storage of the device can be enhanced by adding the CNT layer on the Ny66-Ag thread; however, that could reduce the photovoltaic performance remarkably due to the lower work function of the coated electrode. Moreover, the fabricated device showed significant improvement in the photovoltaic performance after adding the ZnO NWs. The test results after washing the sample proved the advantages of using such device structure in wearable electronics. Further studies on the stability and photovoltaic performance of the device is suggested prior to the practical applications.

4 | EXPERIMENTAL SECTION

4.1 | Materials

The required chemical materials, including PVA (Mw 89 000-98 000, 99+% hydrolyzed) and phosphoric acid (H_3PO_4) (85 wt. % in H2O), ammonium persulfate ($[NH_4]_2S_2O_8$) (APS) (≥98.0%), aniline (ANI) (99%), sodium dodecylbenzenesulfonate (SDBS) (technical grade), zinc acetate dihydrate (ZAD) (≥99.0%), sodium hydroxide (NaOH) (≥98.0%), ethanol, hexamethylenetetramine

10991 14x, 2022, 12, Downloaded from https://onlinelibrary.wiley.com/doi/10.1002/er.8371 by Health Science Center, Wiley Online Library on [15/01/2023]. See the Terms and Conditions (https://onlinelibrary.wiley.com/terms-and-conditions) on Wiley Online Library for rules of use; OA articles are governed by the applicable Creative Commons License

(HMTA) (≥99.0%), and ammonium hydroxide (NH_4OH) (28.0%-30.0% NH_3 basis) were purchased from Sigma-Aldrich and were used as received. Multi-walled CNTs and zinc nitrate hexahydrate (ZNH) (99.0%) were purchased from Alfa Aesar. Silver-coated nylon 66 (Ny66-Ag) conductive thread with a lineal resistance of 50 $\Omega\ m^{-1}$ and SS-based threads were purchased from Jameco Electronics and Electronics123 respectively.

4.2 | Preparation of the gel electrolyte and the CNT ink

The composite gel electrolyte was prepared as was described in our earlier work.[21] The process included three steps starting with adding 3 g of PVA to 2 mL of H_3PO_4 mixed with 20 mL of DI water and stirring well on a hot plate at 90°C over a period of 5 h at a speed of 400 rpm until the PVA was completely solubilized. In the second step, 5 mL solution of 0.1 M APS in 0.5 mL of H_3PO_4 was added to the PVA/H_3PO_4 solution at room temperature with continuous stirring for 30 min at 500 rpm. After that, the PVA/PANI composite gel electrolyte was made by adding 0.2 M of aniline to the PVA/H_3PO_4/APS at room temperature with continuous stirring for 12 h. The CNT ink was made as explained before by dispersing 300 mg of MWCNT and 150 mg of SDBS in 30 mL of deionized (DI) water under probe sonication for 40 min at a power of 30 W and an energy of 40 J.[40]

4.3 | Preparation of electrodes

Three different anode electrodes were fabricated using Ny66-Ag conductive thread as the base: (a) as-purchased Ny66-Ag, (b) CNT coated Ny66-Ag thread (Ny66-Ag/CNT), and (c) ZnO NWs grown on the CNT coated Ny66-Ag (Ny66-Ag/CNT/ZnO-NWs). The Ny66-Ag/CNT electrode was made through repeated, 10 times, dip-coating of Ny66-Ag threads into the CNT ink followed by drying at room temperature. For the Ny66-Ag/CNT/ZnO-NWs electrode, the growth of ZnO nanowires on the Ny66-Ag/CNT thread was carried out through a hydrothermal process that depends on the reactions of zinc acetate dihydrate, zinc nitrate hexahydrate, and hexamethylenetetramine.[41] In brief, the seeding solution (ZnO nanoparticles) was first prepared by dissolving 18 mg of ZAD and 5 mg of NaOH separately into 20 mL of ethanol, followed by adequate stirring on a hotplate at 65°C for 25 min. Then, 20 mL of ethanol was added into the ZAD solution to dilute it, followed by slow stirring at 65°C for 35 min. After the two solutions were brought to the ambient temperature for 30 min, the NaOH solution was slowly added to the ZAD solution using a burette with slow stirring; then, the seeding solution was put into an oven for 2 h to crystallize the ZnO nanoparticles. After the crystallization process, a white precipitate was observed, indicating the existence of ZnO nanoparticles in the seeding solution. In order to provide nucleation sites for the growth process, the Ny66-Ag/CNT thread was dipped into the ZnO seeding solution for 5 min and dried for 5 min at 85°C with repeating the process three times to obtain a uniform layer of ZnO nanoparticles. After the seeding process was done, the growth solution was prepared by dissolving 3 g of ZNH and 0.7 g of HMTA separately into 190 mL of DI water and mixed at room temperature, followed by adding 10 mL of ammonium hydroxide (NH_4OH) to the final mixture to increase the growth efficiency.[42] The Ny66-Ag/CNT/ZnO nanoparticles thread was immersed in the growth solution and put into an oven at 85°C for 8 h, then washed and dried at room temperature. A 3D printed holder was designed and used to set the thread horizontally inside the middle of the growth solution to make the growth rate of the ZnO nanowires uniform around the fibers and reduce unwanted deposits during the hydrothermal process (Figure S4).

4.4 | Characterizations

Surface morphologies and structures of the anode electrodes were characterized via SEM and EDS (HITACHI S-800). VersaSTAT 4 Potentiostat/Galvanostat was used to conduct the electrical and electrochemical experiments in a two-electrode configuration. Different experiments were executed to characterize the electrochemical properties and test the performance of the fiber-shaped hybrid device, including CV, galvanostatic charge-discharge, OCP, SCC, and EIS experiments. To test the fiber-shaped hybrid device under two operation modes (dark and light) and minimize stray light effects in the experiments, the devices were placed in a dark box with an optical fiber connected to a solar simulator (Radiant Source Technology Inc.) with a light intensity of 80 mW cm^{-2} and AM 1.0 interior optical filter.

ACKNOWLEDGEMENTS

This work was supported by the National Science Foundation through NSF 1953089.

CONFLICT OF INTEREST

The authors declare no conflict of interest.

10991114x, 2022, 12, Downloaded from https://onlinelibrary.wiley.com/doi/10.1002/er.8371 by Health Science Center, Wiley Online Library on [15/01/2023]. See the Terms and Conditions (https://onlinelibrary.wiley.com/terms-and-conditions) on Wiley Online Library for rules of use; OA articles are governed by the applicable Creative Commons License

ORCID

Arash Takshi https://orcid.org/0000-0002-4582-8077

REFERENCES

1. Heo JS, Eom J, Kim YH, Park SK. Recent Progress of textile-based wearable electronics: a comprehensive review of materials, devices, and applications. *Small*. 2018;14:1703034.
2. Chen D, Jiang K, Huang T, Shen G. Recent advances in fiber Supercapacitors: materials, device configurations, and applications. *Adv Mater*. 2020;32:1901806.
3. Fakharuddin A, Li H, Di Giacomo F, et al. Fiber-shaped electronic devices. *Adv. Energy Mater.* 2021;11:2101443.
4. Li P, Li J, Zhao Z, et al. A general electrode design strategy for flexible fiber micro-Pseudocapacitors combining ultrahigh energy and power delivery. *Adv Sci*. 2017;4:1700003.
5. Liu W, Liu N, Shi Y, et al. A wire-shaped flexible asymmetric supercapacitor based on carbon fiber coated with a metal oxide and a polymer. *J Mater Chem A*. 2015;3:13461-13467.
6. Cheng X, Zhang J, Ren J, et al. Design of a Hierarchical Ternary Hybrid for a fiber-shaped asymmetric Supercapacitor with high volumetric energy density. *J Phys Chem C*. 2016;120:9685-9691.
7. Chen X, Qiu L, Ren J, et al. Novel electric double-layer capacitor with a coaxial fiber structure. *Adv Mater*. 2013;25:6436-6441.
8. Shen C, Xie Y, Sanghadasa M, et al. Ultrathin coaxial fiber Supercapacitors achieving high energy and power densities. *Mater Interfaces*. 2017;9:39391-39398.
9. Qu G, Cheng J, Li X, et al. A fiber Supercapacitor with high energy density based on hollow graphene/conducting polymer fiber electrode. *Adv Mater*. 2016;28:3646-3652.
10. Yu D, Qian Q, Wei L, et al. Emergence of fiber supercapacitors. *Chem Soc Rev*. 2015;44:647-662.
11. Fu X, Sun H, Xie S, et al. A fiber-shaped solar cell showing a record power conversion efficiency of 10%. *J Mater Chem A*. 2018;6:45-51.
12. Liu G, Gao X, Wang H, et al. A novel photoanode with high flexibility for fiber-shaped dye sensitized solar cells. *J Mater Chem A*. 2016;4:5925-5931.
13. Dong B, Hu J, Xiao X, et al. High-efficiency fiber-shaped perovskite solar cell by vapor-assisted deposition with a record efficiency of 10.79%. *Adv Mater Technol*. 2019;4:1900131.
14. Liu D, Zhao M, Li Y, et al. Solid-state, polymer-based fiber solar cells with carbon nanotube electrodes. *ACS Nano*. 2012;6:11027-11034.
15. Hatamvand M, Kamrani E, Lira-Cantú M, et al. Recent advances in fiber-shaped and planar-shaped textile solar cells. *Nano Energy*. 2020;71:104609.
16. Pan S, Lin H, Deng J, et al. Novel wearable energy devices based on aligned carbon nanotube fiber textiles. *Adv Energy Mater*. 2015;5:1401438.
17. Liu K, Chen Z, Lv T, et al. A self-supported graphene/carbon nanotube hollow fiber for integrated energy conversion and storage. *Nano-Micro Lett*. 2020;12:64.
18. Liang J, Zhu G, Wang C, et al. MoS2-based all-purpose fibrous electrode and self-powering energy fiber for efficient energy harvesting and storage. *Adv Energy Mater*. 2017;7:1601208.
19. Chen X, Sun H, Yang Z, et al. A novel "energy fiber" by coaxially integrating dye-sensitized solar cell and electrochemical capacitor. *J Mater Chem A*. 1897;2014:2-1902.
20. Chai Z, Zhang N, Sun P, et al. Tailorable and wearable textile devices for solar energy harvesting and simultaneous storage. *ACS Nano*. 2016;10:9201-9207.
21. Aljafari B, Indrakar SK, Ram MK, Biswas PK, Stefanakos E, Takshi A. Tailorable and wearable textile devices for solar energy harvesting and simultaneous storage. *Chem Electro Chem*. 2019;6:5888.
22. Kareri T, Aljafari B, Takshi A. A Polyaniline-Based Redox-Active Composite Gel Electrolyte with Photo-Electric and Electrochromic Properties. *Int Soc Opt Photonics*. 2020;11496:8-14.
23. Kareri T, Aljafari B, Takshi A. Hybrid photovoltaic-supercapacitors: effect of the counter electrode on the device performance. *Int Soc Opt Photonics*. 2021;11824:22-27.
24. Kareri T, Yadav RL, Takshi A. Image processing analysis of supercapacitors with twisted fiber structures and a gel electrolyte. *J Appl Electrochem*. 2022;52:139-148.
25. Guerra A, Achour A, Vizireanu S, et al. ZnO/carbon nanowalls shell/core nanostructures as electrodes for supercapacitors. *Appl Surf Sci*. 2019;481:926-932.
26. Chodankar NR, Pham HD, Nanjundan AK, et al. True meaning of Pseudocapacitors and their performance metrics: asymmetric vs hybrid Supercapacitors. *Small*. 2020;16:2002806.
27. Takshi A, Aljafari B, Kareri T, Stefanakos E. A critical review on the voltage requirement in hybrid cells with solar energy harvesting and energy storage capability. *Batteries Supercaps*. 2021;4:252-267.
28. Takshi A, Yaghoubi H, Tevi T, Bakhshi S. Photoactive supercapacitors for solar energy harvesting and storage. *J Power Sources*. 2015;275:621-626.
29. Juan B, Garcia-Belmonte G. On voltage, Photovoltage, and photocurrent in bulk heterojunction organic solar cells. *J Phys Chem Lett*. 2011;2:1950-1964.
30. Ram MK, Goswami DY, Takshi A, Stefanakos E. A new chromic (TouchChromic) thin film. *Acta Mater*. 2016;121:325-330.
31. Qiu L, Deng J, Lu X, Yang Z, Peng H. Integrating perovskite solar cells into a flexible fiber. *Angew Chem Int Ed*. 2014;53:10425-10428.
32. White M-S, Olson D, Shaheen S, Kopidakis N, Ginley DS. Inverted bulk-heterojunction organic photovoltaic device using a solution-derived ZnO underlayer. *Appl Phys Lett*. 2006;89:143517.
33. Georgousis G, Kontou E, Kyritsis A, Pissis P, Mičušík M, Omastová M. Piezoresistivity of conductive polymer nanocomposites: experiment and modeling. *J Reinf Plast Compos*. 2018;37:1085-1098.
34. Shiraishi M, Ata M. Work function of carbon nanotubes. *Carbon*. 1913;2001:39.
35. Gao R, Pan Z, Wang ZL. Work function at the tips of multiwalled carbon nanotubes. *Appl Phys Lett*. 2001;78:1757-1759.
36. EmraháUnalan H. Flexible organic photovoltaics from zinc oxide nanowires grown on transparent and conducting single walled carbon nanotube thin films. *J Mater Chem*. 2008;18:5909.
37. Dong Y, Zou Y, Song J, Zhu Z, Li J, Zeng H. Self-powered fiber-shaped wearable omnidirectional photodetectors. *Nano Energy*. 2016;30:173-179.

10991 14x, 2022, 12, Downloaded from https://onlinelibrary.wiley.com/doi/10.1002/er.8371 by Health Science Center, Wiley Online Library on [15/01/2023]. See the Terms and Conditions (https://onlinelibrary.wiley.com/terms-and-conditions) on Wiley Online Library for rules of use; OA articles are governed by the applicable Creative Commons License

38. Xiang X-B, Yu Y, Wen W, Wu J-M. Construction of hierarchical ag@TiO2@ZnO nanowires with high photocatalytic activity. *New J Chem*. 2018;42:265-271.
39. Wibowo A, Marsudi MA, Amal MI, et al. ZnO nanostructured materials for emerging solar cell applications. *RSC Adv*. 2020; 10:42838-42859.
40. Rahimi F, Takshi A. Energy storage capability of the dye sensitized solar cells via utilization of highly porous carbon electrodes. *Int Soc Opt Photonics*. 2016;9937:146-152.
41. Zhao C, Li X, Wu Q, Liu X. A thread-based wearable sweat nanobiosensor. *Biosens Bioelectron*. 2021;188:113270.
42. Li X, Zhao C, Liu X. A paper-based microfluidic biosensor integrating zinc oxide nanowires for electrochemical glucose detection. *Microsyst Nanoeng*. 2015;1:1.

SUPPORTING INFORMATION

Additional supporting information can be found online in the Supporting Information section at the end of this article.

How to cite this article: Kareri T, Hossain MS, Ram MK, Takshi A. A flexible fiber-shaped hybrid cell with a photoactive gel electrolyte for concurrent solar energy harvesting and charge storage. *Int J Energy Res*. 2022;46(12):17084-17095. doi:10.1002/er.8371

10991114x, 2022, 12, Downloaded from https://onlinelibrary.wiley.com/doi/10.1002/er.8371 by Health Science Center, Wiley Online Library on [15/01/2023]. See the Terms and Conditions (https://onlinelibrary.wiley.com/terms-and-conditions) on Wiley Online Library for rules of use; OA articles are governed by the applicable Creative Commons License